



## Search for Standard Model Higgs Boson Production in Association with a $W^\pm$ Boson with $9.45 \text{ fb}^{-1}$ of CDF Data

The CDF Collaboration  
URL <http://www-cdf.fnal.gov>  
(Dated: March 7, 2012)

We present a search for the standard model Higgs boson produced in association with a  $W^\pm$  boson. This search uses data corresponding to an integrated luminosity of  $9.45 \text{ fb}^{-1}$  collected by the CDF detector at the Tevatron. We select  $WH \rightarrow \ell\nu b\bar{b}$  candidate events with two jets, large missing transverse energy, and exactly one charged lepton from the central or forward regions of the detector. We further require that at least one jet be identified to originate from a bottom quark. Discrimination between the Higgs boson signal and the comparatively large backgrounds is improved through the use of a Bayesian artificial neural network. The number of tagged events and the resulting neural network output distributions are consistent with the standard model expectations. We see a small broad excess for signal-like events and set 95% confidence level upper limits on the  $WH$  production cross section times the branching ratio to decay to  $b\bar{b}$  pairs,  $\sigma(p\bar{p} \rightarrow W^\pm H) \times BR(H \rightarrow b\bar{b})$ . For the mass range of  $90 \text{ GeV}/c^2$  through  $150 \text{ GeV}/c^2$  with  $5 \text{ GeV}/c^2$  mass increments we set observed (expected) upper limits from  $1.38$  ( $1.36$ )  $\times$  SM through  $21.7$  ( $15.9$ )  $\times$  SM. For  $115 \text{ GeV}/c^2$  the upper limit is  $3.13$  ( $1.97$ ). The increase in sensitivity over the previous version of this analysis is  $\sim 32\%$  at  $115 \text{ GeV}/c^2$ , out of which  $\sim 11\%$  is due to the extra integrated luminosity and the rest of the gain is due to improved analysis techniques.

*Preliminary Results for Winter 2012 Conferences*

## I. INTRODUCTION

The Higgs boson is the only elementary particle predicted by the standard model (SM) of elementary particles and their interactions that has not been confirmed by experiments. It is predicted by the Higgs mechanism in order to explain the spontaneous symmetry breaking and the origin of mass for the electroweak gauge bosons and the fermions. If the Higgs boson is observed experimentally, it will confirm the SM and the Higgs mechanism. If it is confirmed not to exist, another model will have to be identified to describe correctly the spontaneous symmetry breaking observed in nature.

We perform a search for the SM Higgs boson using data collected by the Collider Detector at Fermilab at the Tevatron with an integrated luminosity of  $9.45 \text{ fb}^{-1}$ . The Large Electron Positron Collider (LEP) has excluded Higgs boson masses below  $114.4 \text{ GeV}/c^2$  [1], and the LHC experiments, ATLAS and CMS, have now limited the SM Higgs boson to have mass between  $115.5$  and  $127 \text{ GeV}/c^2$  [2, 3]. Clearly, the search for low-mass Higgs boson is well motivated. For low Higgs boson masses (below  $135 \text{ GeV}/c^2$ ), the dominant decay mode is  $H \rightarrow b\bar{b}$ . The dominant production mode at the Tevatron is gluon fusion producing one Higgs boson and nothing else. Since the desired Higgs boson decays to a bottom-antibottom quark pair, the signal could not be distinguished from the SM bottom quark pair production, which is produced with a rate nine orders of magnitude higher. For this reason, we consider the next most abundant Higgs boson production mechanism at the Tevatron, namely the associated production of a Higgs boson with a  $W$  boson, also called Higgsstrahlung, since a virtual  $W$  boson radiates a Higgs boson [4]. In this analysis, we select  $WH \rightarrow \ell\nu b\bar{b}$  candidate events with a charged lepton, missing transverse energy and two jets originating from bottom quarks. The selection of a charged lepton reduces greatly the background fraction in the sample. We also include the signal contribution of  $ZH \rightarrow \ell\ell b\bar{b}$ , where one of the charged leptons escapes detection, which adds about 3% more signal. Furthermore, we use complementary high- $p_T$  lepton and missing transverse energy ( $\cancel{E}_T$ ) triggers to maximize our signal acceptance.

The latest  $WH$  search from CDF [5] was presented at EPS 2011 and was performed using a dataset with an integrated luminosity of  $7.5 \text{ fb}^{-1}$ , which is 21% smaller than the current analysis dataset. Just as in the latest analysis, the current analysis employs a Bayesian artificial neural network (BNN) discriminant [6] to improve discrimination between signal and background. However, the current analysis embodies improvements. The most important one is the use of a more sophisticated algorithm to tag jets originating from a  $b$  quark. Moreover, the signal acceptance has been increased by considering an inclusive set of triggers, in which efficiency is determined using neural-network regression. In addition, for the first time, this analysis employs a BNN discriminant for events with three jets.

## II. DATA SAMPLE & EVENT SELECTION

### A. Triggers

We use charged lepton,  $\cancel{E}_T + \text{jets}$ , and  $\cancel{E}_T$  triggered data collected through September 2011 and corresponding to an integrated luminosity of  $9.45 \text{ fb}^{-1}$ . The events are collected by the CDF II detector and classified according to their trigger type.

Central lepton events enter the analysis from high- $p_T$  electron or muon triggers that have an  $18 \text{ GeV}$  threshold [7]. Some candidates that fail the standard electron reconstruction are recovered if they are deemed to be electron-like according to a multivariate likelihood method (loose electron-like leptons). In addition to the primary lepton triggers, for the first time a suite of additional lepton-based triggers are included. The inclusion of these new triggers improves lepton acceptance by about 10 %.

We select forward (plug) electron events with a trigger intended for  $W$  candidate events. The plug electron trigger requires both a plug electron candidate and missing transverse energy. Plug electron events are further required offline to have  $E_T > 20 \text{ GeV}$  and  $\cancel{E}_T > 25 \text{ GeV}$ .

To select events that have an identified loose (non-triggered) charged lepton, we use one trigger based on  $\cancel{E}_T$  and two triggers based on  $\cancel{E}_T + \text{jets}$ . The efficiencies of the three triggers at each trigger level are parametrized using sigmoid turn-on curves in  $\cancel{E}_T$  [8]. The following trigger-specific offline jet selections are imposed: two jets with  $E_T > 25 \text{ GeV}$ ,  $\Delta R > 1.0$ , and at least one central jet with  $|\eta| < 0.9$  are required for one  $\cancel{E}_T + \text{jets}$ , while in the other  $\cancel{E}_T + \text{jets}$

trigger the presence of two jets with  $E_T > 40$  and  $E_T > 25$  GeV is required. For the  $\cancel{E}_T$  +jets trigger, two jets with  $E_T > 20$  GeV and  $|\eta| < 2.0$  are required.

## B. Event Selection

Offline, central electron or muon candidates are required offline to be isolated and have  $E_T$  (or  $p_T$ )  $> 20$  GeV (GeV/ $c$ ). Since the  $W$ +jets signature presents a large missing transverse energy, we require  $\cancel{E}_T > 20$  GeV ( $\cancel{E}_T > 10$  GeV) for electrons (muons).

We consider different types of loose muon candidates that are primarily from the  $W \rightarrow \mu\nu$  decay where the muon failed the standard identification or entered into a detector gap region. Some of these lepton candidates are taken from the extended muon coverage (EMC) [9]. Isolated tracks that have  $p_T > 20$  GeV, are isolated from other track activity in the event, and that do not belong to any of the EMC categories, are also selected and included in the category of loose muons. Isolated tracks with significant deposits of energy in the calorimeter are also selected and included in the category of loose electron-like leptons. These lepton candidates originate primarily from leptonic decays of  $W$  bosons, where the electrons fail the standard identification, or from  $\tau$  lepton decays in a single charged hadron (one-prong).

We increase the purity of the sample by applying cuts intended to remove multijet events due to QCD processes that include fake-lepton signatures. The QCD veto is based on the SVM multivariate technique, which uses different kinematical input variables [10]. Some of them are related to the  $W$  kinematics like the lepton  $p_T$ ,  $\cancel{E}_T$ , or  $\Delta\phi(\text{lepton, } E_T^{\text{uncorrected}})$ . Some are related to the kinematics of the jets in the event like  $\cancel{E}_T^{\text{uncorrected}}$  and the transverse energy of the second leading  $E_T$  jet. A variable denoted as  $\cancel{E}_T$  significance is also used. This variable is defined as the ratio of  $\cancel{E}_T$  to a weighted sum of factors correlated with mismeasurement, such as angles between the  $\cancel{E}_T$  and the jets and the amount of jet energy corrections.

For forward electrons and loose electron-like leptons the cut-based QCD veto used in previous iterations of this analysis is used [11]. This veto applies a linear cut on the  $\cancel{E}_T$  and the azimuthal angle ( $\phi$ ) between the  $\cancel{E}_T$  and each of the jets ( $\cancel{E}_T > 45 - (30 \cdot |\Delta\phi|)$  GeV), requires a large transverse mass of the reconstructed  $W$  boson candidate ( $M_T(W) > 20$  GeV), and a large  $\cancel{E}_T$  significance.

The events from all trigger types are classified according to the number of jets having  $E_T > 20$  GeV and  $|\eta| < 2.0$ . Events that have exactly two or three jets are selected, while events with a different number of jets are used as control regions. Because the Higgs boson decays to  $b\bar{b}$  pairs, we employ  $b$ -tagging algorithms that rely on the relatively long lifetime and large mass of the  $b$  quark. A new  $b$ -tagging algorithm denoted as The Higgs-Optimized  $b$ -Identification Tagger (HOBIT) [12] is used in the current analysis. We require at least one of the jets in the event to be tagged by HOBIT. Details on the  $b$ -tagging algorithms are given in the next section.

## C. Bottom Quark Tagging Algorithms

To reduce considerably the backgrounds to this Higgs boson search, we require that at least one jet in the event be identified as originating from a  $b$  quark by the HOBIT algorithm. It is a multivariate  $b$ -tagger that has been optimized to identify  $b$ -jets from the decay of Higgs bosons. HOBIT produces a continuous output variable for each candidate  $b$ -jet, which allows the operating point to be chosen to obtain the best Higgs boson sensitivity for a given analysis. The HOBIT tagger uses input variables from the RomaNN [13] and BNess [14] taggers. HOBIT output values range between -1 and 1, where a value of -1 indicates that a jet is light-jet-like, and a value of 1 indicates that the jet is  $b$ -quark-like. Two operational points of the HOBIT algorithm are used to define the tagging categories. These two operational points correspond to values of the HOBIT output of 0.98, and 0.72, and are denoted as Tight (T) and Loose (L), respectively. Based on them, the following 5 orthogonal  $b$ -tagging categories are defined: TT, TL, LL, T, and L.

### D. Total $WH$ ( $ZH$ ) Acceptance

The signal acceptance is measured in a sample of Monte Carlo events generated with the PYTHIA program [17]. We consider the signal acceptance not only from the  $WH \rightarrow \ell\nu b\bar{b}$  process, but also from  $ZH \rightarrow \ell\ell b\bar{b}$ , with one undetected charged lepton. The detection efficiency for the signal events is defined as

$$\epsilon_{WH(ZH)\rightarrow\ell\nu b\bar{b}} = \epsilon_{z_0} \cdot \epsilon_{\text{trig}} \cdot \epsilon_{\text{leptonid}} \cdot \epsilon_{WH(ZH)\rightarrow\ell\nu b\bar{b}}^{\text{MC}} \cdot \left( \sum_{\ell=e,\mu,\tau} Br(W \rightarrow \ell\nu(Z \rightarrow \ell\ell)) \right), \quad (1)$$

where  $\epsilon_{WH(ZH)\rightarrow\ell\nu b\bar{b}}^{\text{MC}}$  is the fraction of signal events (with  $|z_0| < 60$  cm) passing the kinematic requirements. The difference in  $b$ -tagging efficiency between data and MC is accounted for by applying scale factors to the tagging efficiency in the MC. The quantity  $\epsilon_{z_0}$  is the efficiency of the  $|z_0| < 60$  cm cut,  $\epsilon_{\text{trig}}$  is the trigger efficiency;  $\epsilon_{\text{leptonid}}$  is the efficiency to identify a lepton;  $\epsilon_{\text{iso}}$  is the efficiency of the energy isolation cut; and  $Br(W \rightarrow \ell\nu(Z \rightarrow \ell\ell))$  is the branching ratio for leptonic  $W(Z)$  decay. For plug electrons,  $\epsilon_{\text{trig}}$  is parametrized as a function of the trigger missing transverse energy and the  $E_T$  of the electron.

### III. BACKGROUNDS

This analysis builds on the method of background estimation detailed in Ref. [15]. In particular, the contributions from the following individual backgrounds are calculated: falsely  $b$ -tagged events,  $W$  production with heavy flavor quark pairs, multijet events with false  $W$  (non- $W$ ) signatures, top quark production, and diboson production.

We estimate the amount of falsely  $b$ -tagged events (mistags) from the number of pretag  $W +$  light flavor events. The amount of pretag  $W +$  light flavor is determined by a fit of the pretag  $\cancel{E}_T$  distribution to  $W$  and non- $W$  templates. To estimate the amount of  $W +$  light flavor in the tagged sample, we apply a per-jet false tag rate parametrization (mistag matrix) to the pretag  $W +$  light flavor events.

The number of events from  $W +$  heavy flavor is calculated using information from both data and Monte Carlo programs. We calculate the fraction of  $W$  events with associated heavy flavor production in the ALPGEN Monte Carlo program interfaced with the PYTHIA parton shower code [17, 18]. This fraction and the tagging efficiency for such events are applied to the number of events in the original  $W$ +jets sample after correcting for the  $t\bar{t}$  and electroweak contributions.

We use the  $\cancel{E}_T$  shape difference between the non- $W$  and the other background models to constrain the amount of QCD events. We perform a likelihood fit to the  $\cancel{E}_T$  distribution to determine the total amount of QCD. We deduce the QCD fraction in the signal region by integrating the fitted distributions above our  $\cancel{E}_T$  cut (25 GeV for plug electrons, 10 GeV for the central muons, namely CMUP and CMX, and 20 GeV for all other leptons). We estimate the non- $W$  contribution to the tagged sample by fitting the  $\cancel{E}_T$  distribution of the tagged events.

The summary of the background contributions, signal expectation and data yield is shown in Table I.

### IV. SYSTEMATIC UNCERTAINTIES

The  $b$ -tagging uncertainty is dominated by the uncertainty on the data/MC scale factors. This uncertainty is evaluated separately for the Tight and Loose operational points of the  $b$ -tagger. The rate uncertainties due to this effect for the different  $b$ -tagging categories are summarized in Table II. The uncertainties due to initial- and final-state radiation are estimated by changing the parameters related to ISR and FSR, halving and doubling the default values. The difference from the nominal acceptance is taken as the systematic uncertainty. These uncertainties range from  $\approx 5 - 10\%$  for most of the considered categories. Other uncertainties on parton distribution functions, trigger efficiencies, or lepton identification contribute to a smaller extent to the overall uncertainty. The lepton reconstruction and trigger efficiency uncertainties are more important for loose muons and loose electron-like leptons, their values are around 4.5% for the lepton reconstruction and around 3% for the trigger efficiency. For central tight leptons and plug electrons

Number of Jets	2 jets					3 jets	
Tagging categories	TT	TL	T	LL	L	TT	TL
DiTop	177.49±22.17	211.19±19.8	544.5±52.06	63.04±6.93	327.74±33.71	495.7±61.59	581.77±54.47
STopS	59.1±7.06	66.39±5.85	118.38±10.68	19.35±2.19	69.4±7.13	19.34±2.33	22.66±2.01
STopT	17.4±2.48	32.45±3.98	228.45±25.63	12.21±1.32	134.83±15.56	22.13±3.03	29.87±3.32
WW	1.9±0.48	15.54±3.13	217.47±27.09	29.26±4.5	719.24±70.55	1.8±0.35	8.04±1.43
WZ	21.86±2.63	25.97±2.28	63.3±6.23	11.8±1	115.13±10.59	4.19±0.51	6±0.57
ZZ	2.6±0.3	2.73±0.24	7.87±0.77	1.08±0.09	11.98±1.08	0.96±0.11	1.22±0.11
Zjets	11.94±1.29	23.24±2.47	184.32±19.71	30.93±3.46	815.82±85.61	7.03±0.75	15.4±1.62
Wbb	284.99±116.78	382.43±155.86	1372.45±559.67	129.59±52.89	948.67±387.04	107.98±45.01	162.42±67.48
Wcc	22.54±9.39	141.43±58.32	1379.5±564.72	196.66±80.63	3332.54±1360.1	12.59±5.31	71.59±30.04
Wlf	5.17±1.54	73.93±16.53	1179.09±191.85	293.49±47.08	9732.87±1094.5	3.21±1.1	41.46±10.51
QCD	12.35±7.94	101.82±41.71	680.92±272.42	125.62±50.72	2031.95±812.95	5.79±5.17	68.53±28.41
Bkg	617.34±172.05	1077.12±309.74	5976.25±1730.5	913.03±250.76	18240.17±3877.7	680.72±125.24	1008.96±200.09
Obs	556	907	5737	865	18606	643	850
WH115	9.57±0.98	9.98±0.62	16.29±1.04	2.7±0.27	9.07±0.75	2.2±0.22	2.41±0.14

TABLE I: Background summary, signal expectation and data yield for the events with two jets in all  $b$ -tagging categories for central leptons.

those two sources of uncertainty are reduced to  $\approx 2\%$  and  $\approx 1\%$ , respectively. The effect of the uncertainty in the jet energy scale (JES) is evaluated by applying jet-energy corrections that describe  $\pm 1\sigma$  variations in the default correction factor. This uncertainty ranges from  $\approx 2 - 10\%$  for most of the considered categories. The uncertainty in the shape of the BNN discriminant due to the JES is also taken into account. Rate and shape systematics are considered for the uncertainty in the renormalization scale used to generate the  $W + \text{jets}$  MC samples by halving and doubling the default value. See Tables IV and V for the full set of systematic uncertainties included in the analysis.

$WH \rightarrow \ell\nu bb, 2\text{jets}$		
CDF Run II Preliminary $9.45 \text{ fb}^{-1}$		
$b$ -tagging category	Tight tag uncertainty	Loose tag uncertainty
TT	7.8%	0
TL	3.9%	3.2%
LL	0%	6.3%
T	3.9%	0
L	0%	6.2%

TABLE II:  $b$ -tagging efficiency systematic uncertainties for the different  $b$ -tagging categories.

## V. BAYESIAN NEURAL NETWORK

To improve further the signal to background discrimination after the event selection, we employ a Bayesian neural network trained on a variety of kinematic variables to distinguish  $WH$  events from the background. For this analysis, we employ distinct BNN discriminant functions that were optimized separately for the different tagging categories in order to increase the sensitivity. Each discriminant is optimized separately for each Higgs boson mass used in the search.

The discriminant used for the TT tag category is trained using 7 input variables. The most sensitive variable  $M_{jj}$ , is the dijet invariant mass and shown on Fig. 1. To improve the dijet mass resolution, we apply neural network based jet energy correction [19]. Another input variable is the  $p_T$  imbalance, which is the difference between the scalar sum of the  $p_T$  of all measured objects and the  $\cancel{E}_T$ . Specifically, it is calculated as  $p_T(\text{jet}_1) + p_T(\text{jet}_2) + p_T(\text{lep}) - \cancel{E}_T$ . The third variable is  $M_{\ell\nu j}^{max}$ , which is the invariant mass of the lepton,  $\cancel{E}_T$ , and one of the two jets, where the jet is chosen to give the maximum invariant mass. The fourth variable is  $Q_{lep} \times \eta_{lep}$ , the electric charge of the charged lepton times the  $\eta$  of the lepton. The fifth variable is the  $\sum E_T$  (loose jets), which is the scalar sum of the loose jet transverse energy. A loose jet is defined as a jet having  $|\eta| < 2.4$ ,  $E_T > 12 \text{ GeV}$  and failing the nominal (tight) jet definition of  $|\eta| < 2.0$ ,  $E_T > 20 \text{ GeV}$ . The sixth variable is the  $p_T(W)$ , which is the transverse momentum of the reconstructed  $W$

CDF II Preliminary 9.4 fb <sup>-1</sup>													
M(H) [GeV/c <sup>2</sup> ]	90	95	100	105	110	115	120	125	130	135	140	145	150
Expected	1.36	1.53	1.44	1.58	1.76	1.97	2.3	2.79	3.59	4.85	6.59	9.91	15.9
Observed	1.38	2.07	1.92	2.36	3.03	3.13	4.33	4.93	6.47	8.51	10.9	14.4	21.7

TABLE III: Observed and expected limits as a function of Higgs boson mass including all lepton types and  $b$ -tagging categories, using events with 2 and 3 jets.

boson candidate, computed as  $\vec{p}_T^*(lep) + \vec{p}_T^*(\nu)$ . The seventh and last variable is  $H_T$ , which is the scalar sum of the transverse energies  $H_T = \Sigma_{jets} E_T + p_T(lep) + \cancel{E}_T$ .

The discriminants used for both the TL and LL tag categories are trained with the same input variables as the TT category, with the following exceptions. The variable  $M_{lvj}^{max}$  is replaced by the variable  $M_{lvj}^{min}$ , which is the invariant mass of the lepton,  $\cancel{E}_T$ , and one of the two jets, where the jet is chosen to give the minimum invariant mass. The variable  $\cancel{E}_T$ , the missing transverse energy, replaces the variable  $p_T$  imbalance. The discriminant used for the T tag and L tag categories are trained with the same input variables as the TT category, with the exception that the variable  $M_{lvj}^{max}$  is replaced by the variable  $\cancel{E}_T$ .

Fig. 2 shows a shape comparison of the BNN output between signal and background MC events for the two most sensitive  $b$ -tagging categories used in the two-jet events: TT (top), and TL (bottom).

In order to increase the WH signal acceptance we consider the events with three jets, where the extra jet comes from initial or final state radiation. In the events with three jets the background is dominated by SM  $t\bar{t}$  and  $Wb\bar{b}$  production. Given the difference in the event topologies, we optimize the event selection for each background type individually. We train two types of BNN: first type,  $BNN_{WH:t\bar{t}}^{out}$ , is trained on  $t\bar{t}$  and WH sample, and the second type,  $BNN_{WH:Wb\bar{b}}^{out}$ , is trained on  $Wb\bar{b}$  and WH sample. As our final discriminant we use  $BNN_{WH:Wb\bar{b}}^{out}$  split into a  $t\bar{t}$  dominated region, defined as  $BNN_{WH:t\bar{t}}^{out} < 0.5$ , and a WH region  $BNN_{WH:t\bar{t}}^{out} \geq 0.5$  as defined in Eq. 2. We consider only TT and TL  $b$ -tagging categories in the events with three jets, and the final discriminants are shown in Fig. 3

$$BNN_{3jet}^{out} = \begin{cases} BNN_{WH:Wb\bar{b}}^{out} & \text{if } BNN_{WH:t\bar{t}}^{out} < 0.5, \\ BNN_{WH:Wb\bar{b}}^{out} + 1 & \text{if } BNN_{WH:t\bar{t}}^{out} \geq 0.5. \end{cases} \quad (2)$$

## VI. RESULTS

No significant excess is apparent in the BNN output distributions. A Bayesian statistical approach using a binned likelihood technique is employed in order to estimate upper limits on Higgs boson production by constraining the number of background events to the estimates within uncertainties. For optimal sensitivity, the search is performed simultaneously in each individual TT, the TL, the LL, the T and L  $b$ -tagging categories.

The combined expected and observed limits for all lepton, jet, and tag categories are shown in Fig. 4 and Table III. The shaded regions represent the one and two sigma probability of fluctuations of the observed limit away from the expected limit based on the distribution of possible background-only experimental outcomes.

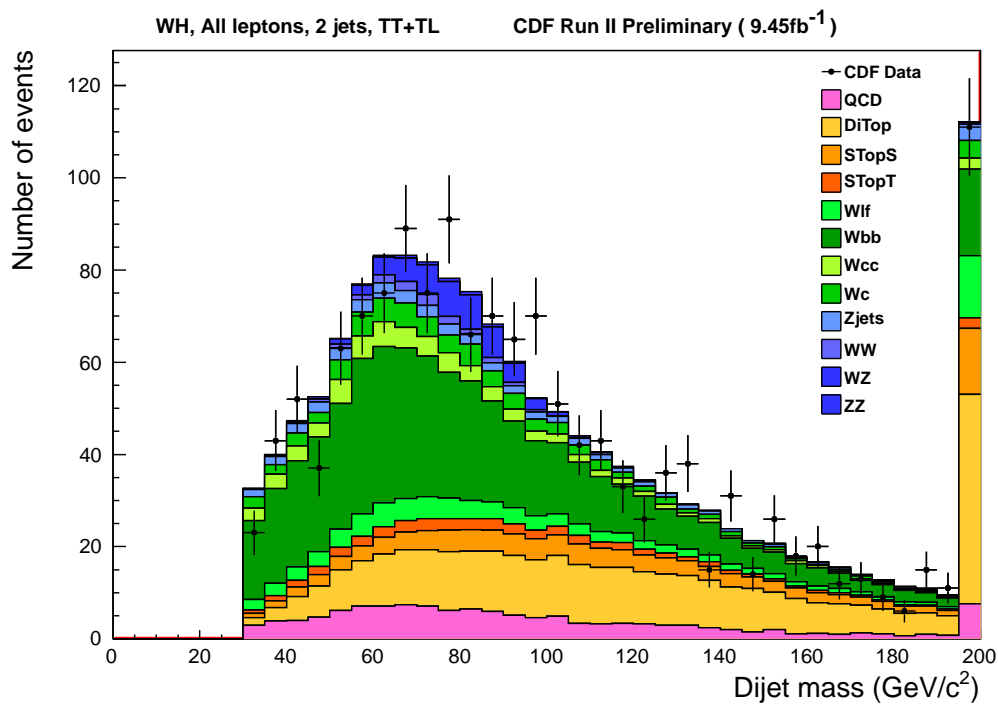


FIG. 1: Predicted and observed dijet invariant mass for the events with two jets in TT and TL combined  $b$ -tagging categories. All lepton types are combined.

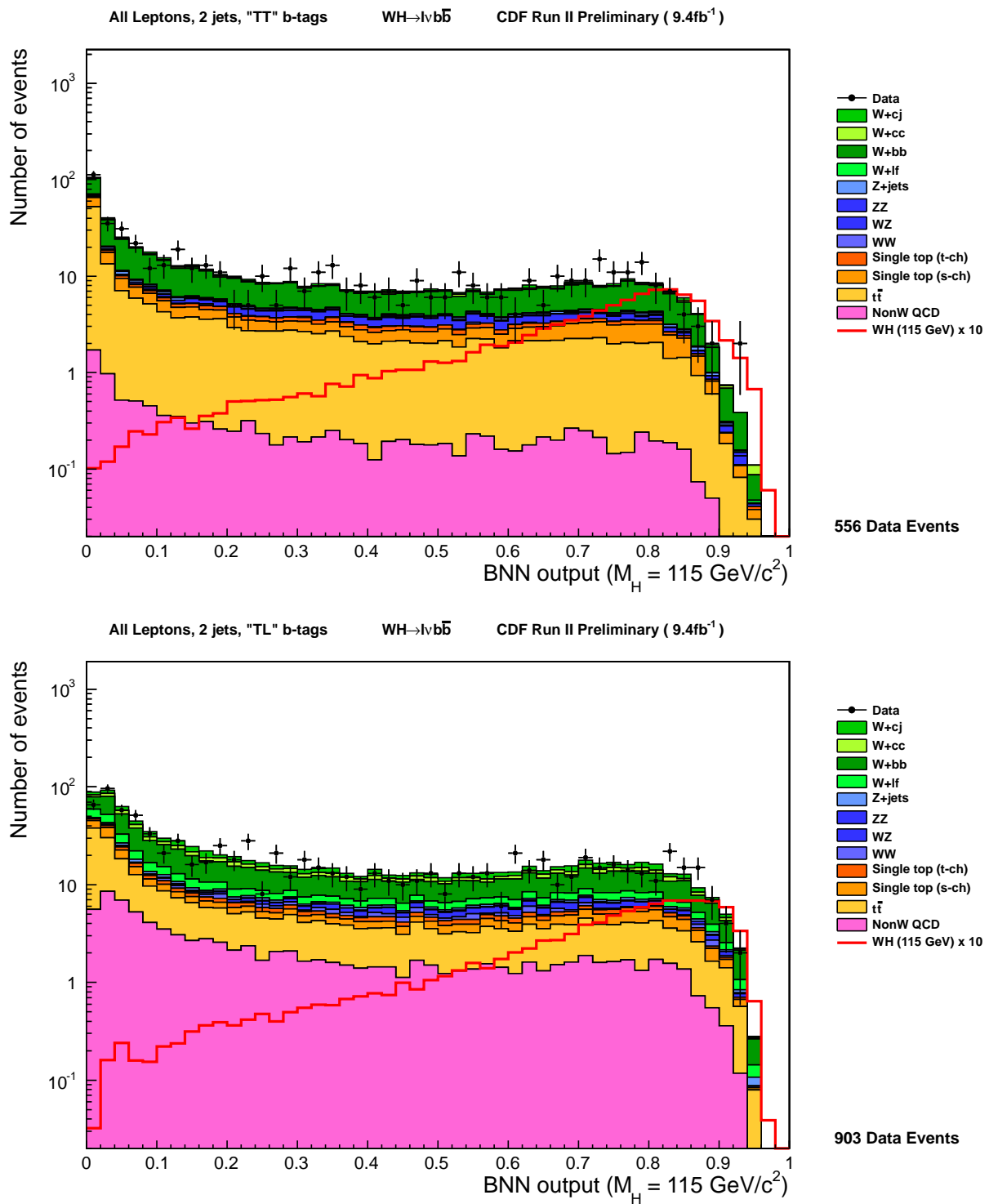


FIG. 2: Predicted and observed output for the neural network trained with a Higgs boson mass of  $115 \text{ GeV}/c^2$  in the events with two jets for the most sensitive  $b$ -tagging categories TT (top), TL (bottom). About 75% of the analysis sensitivity comes from these two categories. All lepton types are combined.

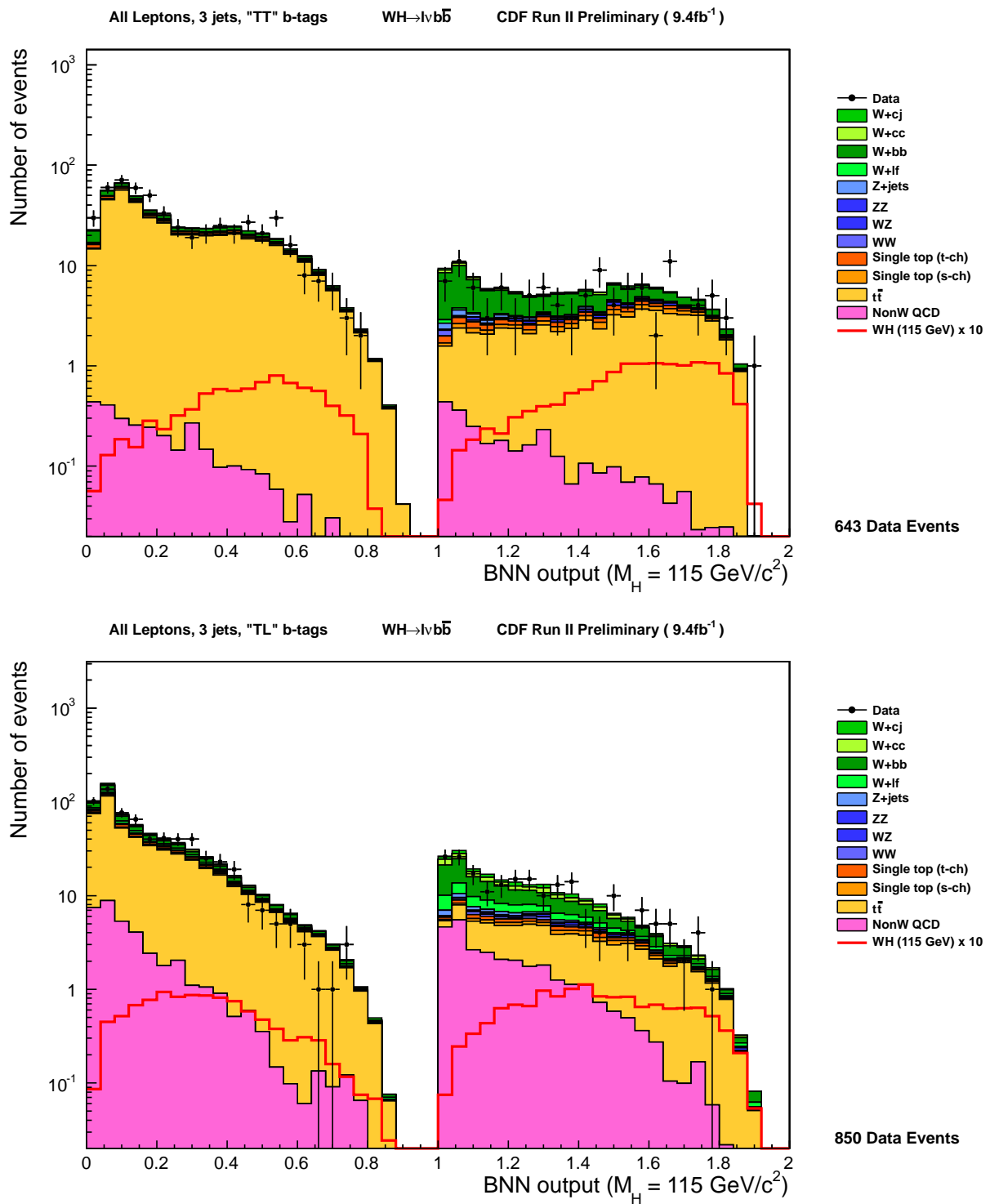


FIG. 3: Predicted and observed output for the neural network trained with a Higgs boson mass of  $115 \text{ GeV}/c^2$  using events with three jets for TT(top) and TL(bottom)  $b$ -tagging categories. All lepton types are combined.

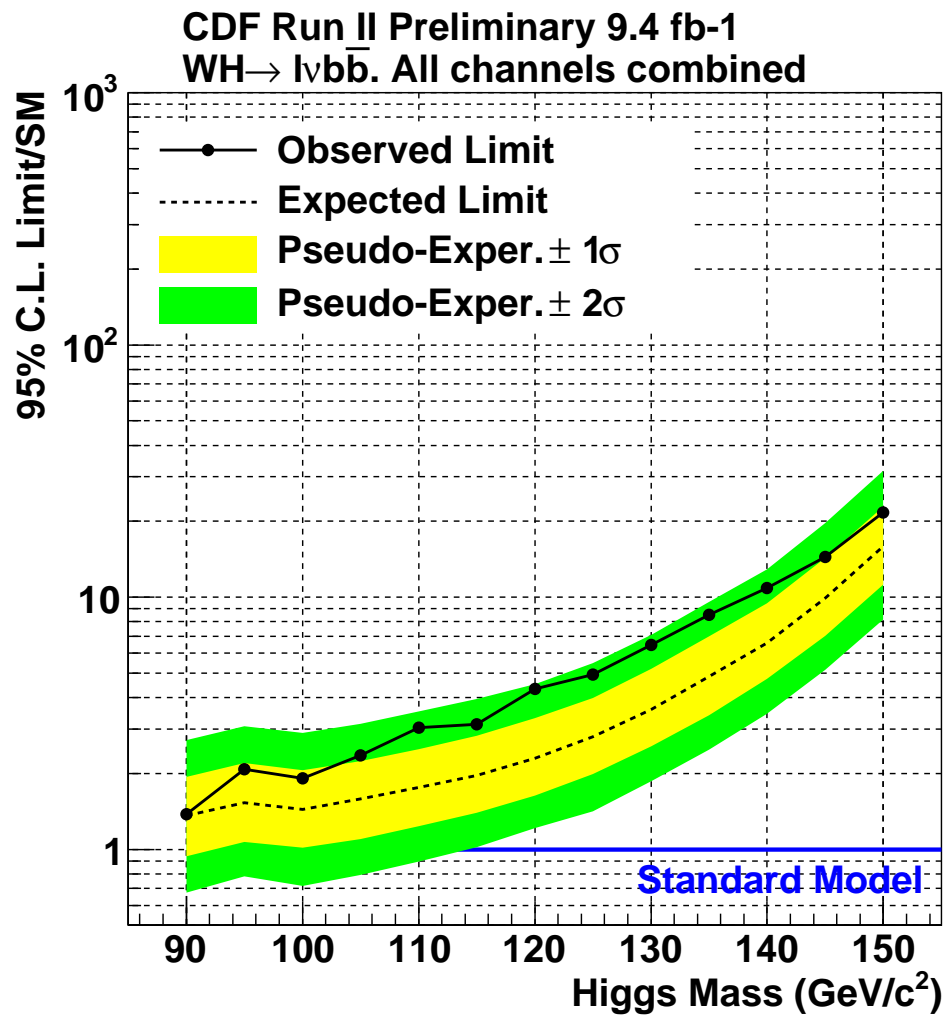


FIG. 4: Expected and observed limits on Higgs boson production and decay for all lepton types and  $b$ -tagging categories in the events with two and three jets, as a function of the Higgs boson mass. The plot shows the expected limit in the units of SM prediction for the Higgs boson cross section.

## VII. CONCLUSIONS

We have presented the results of a search for the standard model Higgs boson decaying to  $b\bar{b}$ , produced in association with a  $W$  boson decaying into a charged lepton and neutrino. We find that for the dataset corresponding to an integrated luminosity of  $9.45 \text{ fb}^{-1}$ , the data agree with the SM background predictions within the systematic uncertainties. However, a small broad excess for signal-like events is evident in the data ( $\lesssim 2$  sigma). We set upper limits on the Higgs boson production cross section times the  $b\bar{b}$  branching ratio. We find that the observed (expected) upper limits  $\sigma(pp \rightarrow W^\pm H) \times \text{Br}(H \rightarrow b\bar{b})$  range from  $1.38$  ( $1.36$ )  $\times \text{SM}$  to  $21.7$  ( $15.9$ )  $\times \text{SM}$  for masses ranging from  $90 \text{ GeV}/c^2$  through  $150 \text{ GeV}/c^2$  with  $5 \text{ GeV}/c^2$  mass increments. For  $115 \text{ GeV}/c^2$  the upper limit is  $3.13$  ( $1.97$ ).

The increase in sensitivity over the previous  $7.5 \text{ fb}^{-1}$  analysis [5] is  $\sim 32\%$  at  $115 \text{ GeV}/c^2$ , out of which  $\sim 11\%$  is due to the extra integrated luminosity and the rest of the gain is due to improved analysis techniques.

## Acknowledgments

We thank the Fermilab staff and the technical staffs of the participating institutions for their vital contributions. This work was supported by the U.S. Department of Energy and National Science Foundation; the Italian Istituto Nazionale di Fisica Nucleare; the Ministry of Education, Culture, Sports, Science and Technology of Japan; the Natural Sciences and Engineering Research Council of Canada; the National Science Council of the Republic of China; the Swiss National Science Foundation; the A.P. Sloan Foundation; the Bundesministerium für Bildung und Forschung, Germany; the Korean World Class University Program, the National Research Foundation of Korea; the Science and Technology Facilities Council and the Royal Society, UK; the Institut National de Physique Nucleaire et Physique des Particules/CNRS; the Russian Foundation for Basic Research; the Ministerio de Ciencia e Innovación, and Programa Consolider-Ingenio 2010, Spain; the Slovak R&D Agency; the Academy of Finland; and the Australian Research Council (ARC).

- 
- [1] R. Barate *et al.* [LEP Working Group for Higgs boson searches], Phys. Lett. B **565**, 61 (2003), [arXiv:hep-ex/0306033]
  - [2] ATLAS Collaboration, Combined search for the Standard Model Higgs Boson using up to  $4.9 \text{ fb}^{-1}$  of pp collision data at  $\sqrt{s} = 7 \text{ TeV}$  with the ATLAS detector at the LHC, ATLAS-CONF-2011-163, arXiv:1202.1408 [hep-ex] (2012).
  - [3] CMS Collaboration, Combined results of searches for the standard model Higgs boson in pp collisions at  $\sqrt{s} = 7 \text{ TeV}$ , CMS-PAS-HIG-11-032, arXiv:1202.1488 [hep-ex] (2012).
  - [4] T. Han and S. Willenbrock, Phys. Lett. **B273** (1991) 167;  
A. Djouadi, J. Kalinowski, and M. Spira, Comp. Phys. Commun. **108 C** (1998) 56.
  - [5] T. Aaltonen *et al.* (CDF Collaboration), CDF Public Note 10596 (2011).
  - [6] <http://www.cs.utoronto.ca/~radford/fbm.software.html>
  - [7] F. Abe *et al.*, Nucl. Instrum. Methods Phys. Res. A **271**, 387 (1988);  
D. Amidei *et al.*, Nucl. Instrum. Methods Phys. Res. A **350**, 73 (1994);  
F. Abe *et al.*, Phys. Rev. D **52**, 4784 (1995);  
P. Azzi *et al.*, Nucl. Instrum. Methods Phys. Res. A **360**, 137 (1995);  
The CDF II Detector Technical Design Report, Fermilab-Pub-96/390-E.
  - [8] A. Buzatu, FERMILAB-THESIS-2011-24, arXiv:1110.5349 (2011).
  - [9] B. Casal, FERMILAB-THESIS-2009-21 (2009).
  - [10] F. Sforza, V. Lippi, G. Chiarelli, J. Phys.: Conf. Ser. **331** 032045 (2011).
  - [11] F. Abe *et al.*, Phys. Rev. D **82**, 112005 (2010);
  - [12] T. Aaltonen *et al.* (CDF Collaboration), CDF Public Note 10803 (2011).
  - [13] C. Ferrazza, D. Jeans, A new b and c jet identification algorithm, CDF Public Note 8451.
  - [14] J. Freeman, W. Ketchum, S. Poprocki, S. Pronko, V. Rusu, P. Wittich, Search for WZ/ZZ in MET+bb channel, CDF Note 10204.
  - [15] A. Abulencia *et al.*, Phys. Rev. **D71**, 072005 (2005).
  - [16] D. Buskulic *et al.* (ALEPH Collaboration), Phys. Lett. B **313**, 535 (1993);  
F. Abe *et al.* (CDF Collaboration), Phys. Rev. D **53**, 1051 (1996);  
A. Affolder *et al.* (CDF Collaboration), Phys. Rev. D **64**, 032002 (2001), Erratum-ibid: Phys. Rev. D **67**, 119901 (2003).
  - [17] P. Edén, C. Friberg, L. Lönnblad, G. Miu, S. Mrenna, E. Norrbin, and T. Sjöstrand, Computer Phys. Commun. **135** (2001) 238.

- [18] M.L. Mangano *et al.*, JHEP 0307:001, 2003.
- [19] T. Aaltonen *et al.*, Improved  $b$ -jet Energy Correction for  $H \rightarrow b\bar{b}$  Searches at CDF, arXiv:1107.3026 (2011).
- [20] T. Aaltonen *et al.* (CDF Collaboration), CDF Public Note 10217 (2011).
- [21] J. M. Campbell and R. K. Ellis, Phys. Rev. D **60**, 113006 (1999) [arXiv:hep-ph/9905386].
- [22] T. Aaltonen *et al.* (CDF Collaboration), CDF Public Note 10805 (2012).

## APPENDIX A: DIBOSON INTERPRETATION

The production of  $WZ$  boson pairs provides an important test of the electroweak sector of the standard model. In addition, the production rate is significantly higher than that for low-mass Higgs boson so a measurement of this process using the tools designed for the Higgs boson search could provide a powerful confirmation of the  $WH \rightarrow \ell\nu b\bar{b}$  analysis. In  $p\bar{p}$  collisions at  $\sqrt{s} = 1.96$  TeV, the next-to-leading order (NLO) SM cross section for this process is  $\sigma(WZ) = 3.2 \pm 0.2$  pb [21]. We perform the diboson analysis using exactly the same event selection and tools as are described above for the  $WH \rightarrow \ell\nu b\bar{b}$  search.

The dijet mass distribution shown in Fig 1 is clearly sensitive to the diboson signal. However, in order to improve sensitivity and to validate the strategy used for  $WH \rightarrow \ell\nu b\bar{b}$  we train a BNN to identify the  $WZ$  signal (see Fig 5).

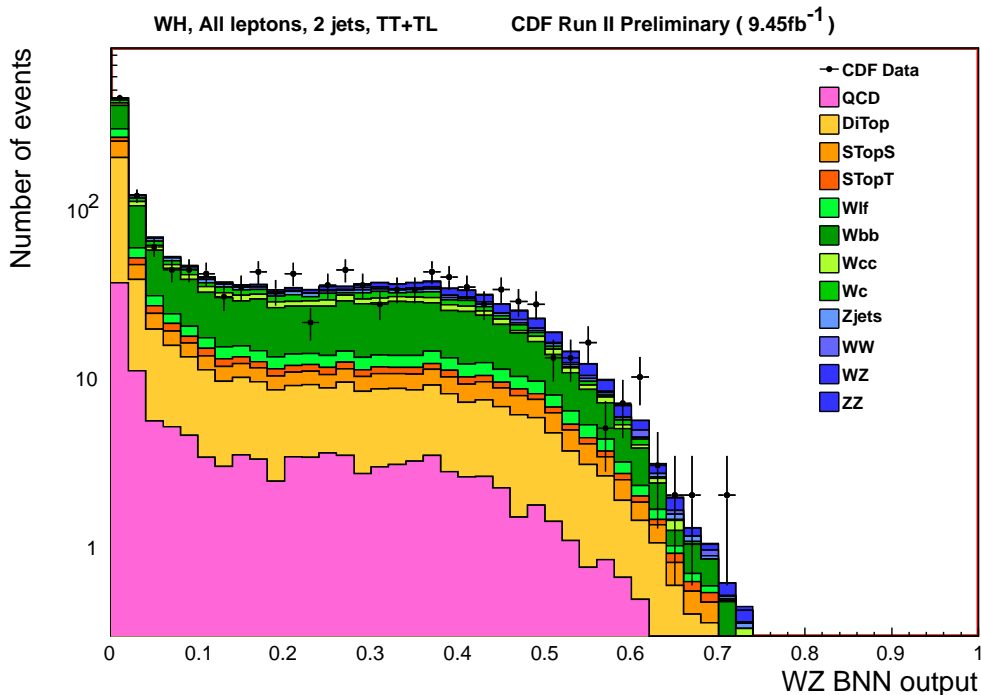


FIG. 5: Predicted and observed diboson-optimized BNN for the events with two jets in TT and TL combined  $b$ -tagging categories. All lepton types are combined.

We fit for the total  $WZ$  cross section distributions which yields  $\sigma(WZ) = 5.63 \pm_{-1.76}^{+1.79}$  pb. We simultaneously fit all of the tag and lepton categories, but only use the two-jet events for this measurement. Fig. 6 shows the posterior distribution from the combined cross section fit [? ]. Although we measure a cross section higher than the SM prediction, the result is still consistent with the NLO SM prediction at within about 1.5 standard deviations.

A diboson combination similar to the CDF Higgs combination is performed with the three main low-mass Higgs analyses and is also found to be consistent with SM predictions [22].

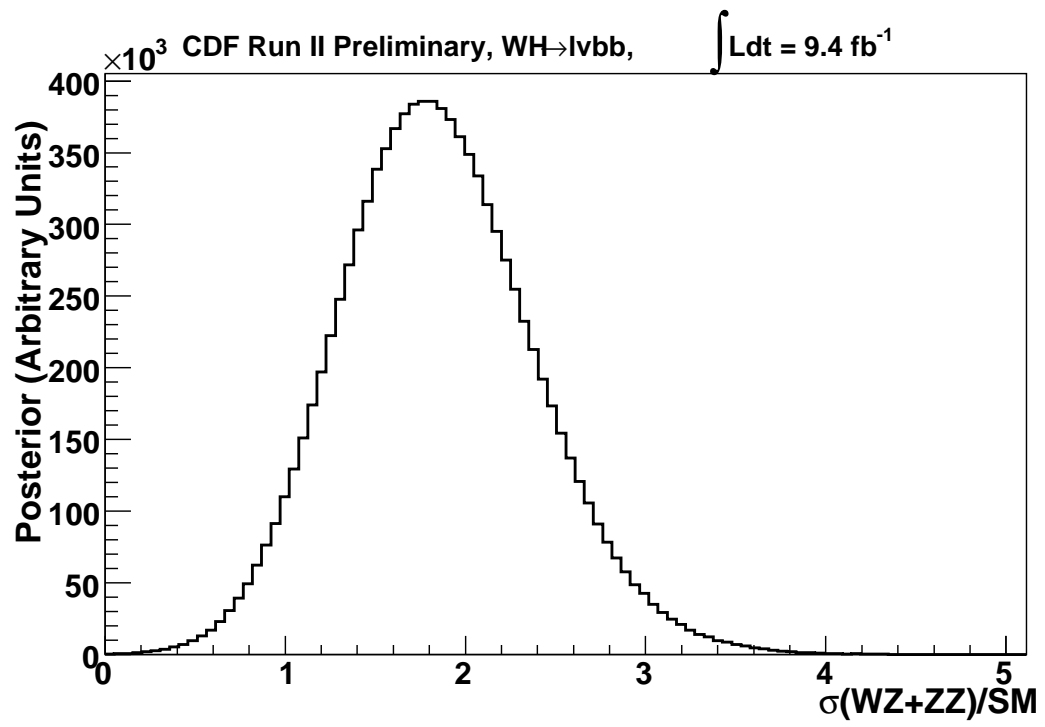


FIG. 6: The posterior curve of the diboson cross section measurement using all tag and lepton categories.

## APPENDIX B: SYSTEMATIC TABLES

TABLE IV: Systematic uncertainties for the CDF  $\ell\nu b\bar{b}$  single tight tag (Tx) and single loose tag (Lx) channels. Systematic uncertainties are listed by name; see the original references for a detailed explanation of their meaning and on how they are derived. Uncertainties are relative, in percent on the event yield. Shape uncertainties are labeled with an “(S)”.

CDF  $\ell\nu b\bar{b}$  single tight tag (Tx) channels relative uncertainties (%)

Contribution	$W+HF$	Mistags	Top	Diboson	Non- $W$	$WH$
Luminosity ( $\sigma_{\text{inel}}(p\bar{p})$ )	3.8	0	3.8	3.8	0	3.8
Luminosity Monitor	4.4	0	4.4	4.4	0	4.4
Lepton ID	2.0-4.5	0	2.0-4.5	2.0-4.5	0	2.0-4.5
Jet Energy Scale	3.2-6.9(S)	0.9-1.8(S)	0.8-9.7(S)	3.6-13.2(S)	0	3.0-5.0(S)
Mistag Rate (tight)	0	19	0	0	0	0
Mistag Rate (loose)	0	0	0	0	0	0
$B$ -Tag Efficiency (tight)	0	0	3.9	3.9	0	3.9
$B$ -Tag Efficiency (loose)	0	0	0	0	0	0
$t\bar{t}$ Cross Section	0	0	10	0	0	0
Diboson Rate	0	0	0	6.0	0	0
Signal Cross Section	0	0	0	0	0	5
HF Fraction in $W$ +jets	30	0	0	0	0	0
ISR+FSR+PDF	0	0	0	0	0	3.8-6.8
$Q^2$	3.2-6.9(S)	0.9-1.8(S)	0	0	0	0
QCD Rate	0	0	0	0	40	0

CDF  $\ell\nu b\bar{b}$  single loose tag (Lx) channels relative uncertainties (%)

Contribution	$W+HF$	Mistags	Top	Diboson	Non- $W$	$WH$
Luminosity ( $\sigma_{\text{inel}}(p\bar{p})$ )	3.8	0	3.8	3.8	0	3.8
Luminosity Monitor	4.4	0	4.4	4.4	0	4.4
Lepton ID	2	0	2	2	0	2
Jet Energy Scale	2.2-6.0(S)	0.9-1.8(S)	1.6-8.6(S)	4.6-9.6(S)	0	3.1-4.8(S)
Mistag Rate (tight)	0	0	0	0	0	0
Mistag Rate (loose)	0	10	0	0	0	0
$B$ -Tag Efficiency (tight)	0	0	0	0	0	0
$B$ -Tag Efficiency (loose)	0	0	3.2	3.2	0	3.2
$t\bar{t}$ Cross Section	0	0	10	0	0	0
Diboson Rate	0	0	0	6.0	0	0
Signal Cross Section	0	0	0	0	0	10
HF Fraction in $W$ +jets	30	0	0	0	0	0
ISR+FSR+PDF	0	0	0	0	0	2.4-4.9
QCD Rate	2.1-6.0(S)	0.9-1.8(S)	0	0	40	0

TABLE V: Systematic uncertainties for the CDF  $\ell\nu b\bar{b}$  double tight tag (TT), one tight tag and one loose tag (TL) and double loose tag (LL) channels. Systematic uncertainties are listed by name; see the original references for a detailed explanation of their meaning and on how they are derived. Uncertainties are relative, in percent on the event yield. Shape uncertainties are labeled with an “(S)”.

CDF  $\ell\nu b\bar{b}$  double tight tag (TT) channels relative uncertainties (%)

Contribution	W+HF	Mistags	Top	Diboson	Non-W	WH
Luminosity ( $\sigma_{\text{inel}}(p\bar{p})$ )	3.8	0	3.8	3.8	0	3.8
Luminosity Monitor	4.4	0	4.4	4.4	0	4.4
Lepton ID	2.0-4.5	0	2.0-4.5	2.0-4.5	0	2.0-4.5
Jet Energy Scale	4.0-16.6(S)	0.9-3.3(S)	0.9-10.4(S)	4.7-19.7(S)	0	2.3-13.6(S)
Mistag Rate (tight)	0	40	0	0	0	0
Mistag Rate (loose)	0	0	0	0	0	0
B-Tag Efficiency (tight)	0	0	7.8	7.8	0	7.8
B-Tag Efficiency (loose)	0	0	0	0	0	0
$t\bar{t}$ Cross Section	0	0	10	0	0	0
Diboson Rate	0	0	0	6.0	0	0
Signal Cross Section	0	0	0	0	0	5
HF Fraction in W+jets	30	0	0	0	0	0
ISR+FSR+PDF	0	0	0	0	0	6.4-12.6
$Q^2$	4.0-8.8(S)	0.9-1.8(S)	0	0	0	0
QCD Rate	0	0	0	0	40	0

CDF  $\ell\nu b\bar{b}$  one tight and one loose tag (TL) channels relative uncertainties (%)

Contribution	W+HF	Mistags	Top	Diboson	Non-W	WH
Luminosity ( $\sigma_{\text{inel}}(p\bar{p})$ )	3.8	0	3.8	3.8	0	3.8
Luminosity Monitor	4.4	0	4.4	4.4	0	4.4
Lepton ID	2.0-4.5	0	2.0-4.5	2.0-4.5	0	2.0-4.5
Jet Energy Scale	3.9-12.4(S)	0.9-3.3(S)	1.4-11.5(S)	5.0-16.0(S)		2.5-16.1(S)
Mistag Rate (tight)	0	19	0	0	0	0
Mistag Rate (loose)	0	10	0	0	0	0
B-Tag Efficiency (tight)	0	0	3.9	3.9	0	3.9
B-Tag Efficiency (loose)	0	0	3.2	3.2	0	3.2
$t\bar{t}$ Cross Section	0	0	10	0	0	0
Diboson Rate	0	0	0	6.0	0	0
Signal Cross Section	0	0	0	0	0	5
HF Fraction in W+jets	30	0	0	0	0	0
ISR+FSR+PDF	0	0	0	0	0	3.3-10.3
$Q^2$	3.9-7.7(S)	0.9-1.9(S)	0	0	0	0
QCD Rate	0	0	0	0	40	0

CDF  $\ell\nu b\bar{b}$  one tight and one loose tag (TL) channels relative uncertainties (%)

Contribution	W+HF	Mistags	Top	Diboson	Non-W	WH
Luminosity ( $\sigma_{\text{inel}}(p\bar{p})$ )	3.8	0	3.8	3.8	0	3.8
Luminosity Monitor	4.4	0	4.4	4.4	0	4.4
Lepton ID	2	0	2	2	0	2
Jet Energy Scale	3.6-6.9(S)	0.9-1.8(S)	1.7-7.9(S)	1.2-8.5	0	2.7-5.4(S)
Mistag Rate (tight)	0	0	0	0	0	0
Mistag Rate (loose)	0	20	0	0	0	0
B-Tag Efficiency (tight)	0	0	0	0	0	0
B-Tag Efficiency (loose)	0	0	6.3	6.3	0	6.3
$t\bar{t}$ Cross Section	0	0	10	0	0	0
Diboson Rate	0	0	0	6.0	0	0
Signal Cross Section	0	0	0	0	0	10
HF Fraction in W+jets	30	0	0	0	0	0
ISR+FSR+PDF	0	0	0	0	0	2.0-13.6
QCD Rate	3.6-6.9(S)	0.9-1.8(S)	0	0	40	0